JACS Au
AN OPEN ACCESS JOURNAL OF THE AMERICAN CHEMICAL SOCIETY

pubs.acs.org/jacsau
Article

Bioinspired Ion Host with Buried and Consecutive Binding Sites for Controlled Ion Dislocation

Wenjie Zhu, Zhenchuang Xu, Wei Zhang, Qi Jia, Haoliang Hao, Yucheng Gu, and Yanchuan Zhao*

Cite This: JACS Au 2024, 4, 4415−4422
Read Online

ACCESS | Metrics & More | Article Recommendations | Supporting Information

ABSTRACT: This study presents a bioinspired ion host featuring continuous binding sites arranged in a tunnel-like structure, closely resembling the selectivity filter of natural ion channels. Our investigation reveals that ions traverse these sites in a controlled, sequential manner due to the structural constraints, effectively mimicking the ion translocation process observed in natural channels. Unlike systems with open binding sites, our model facilitates sequential ion recognition state transitions, enabled by the deliberate design of the tunnel. Notably, we observe dual ion release kinetics, highlighting the system's capacity to maintain ion balance in complex environments and adapt to changing conditions. Additionally, we demonstrate selective binding of two different ions—a challenging task for systems lacking structured tunnels.

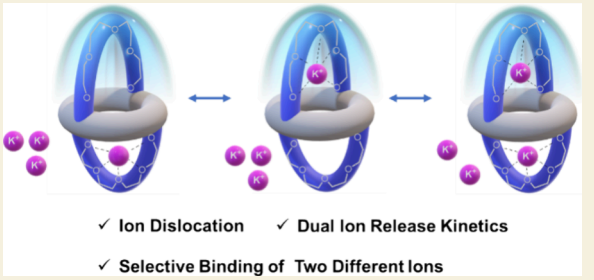

KEYWORDS: *confined space, ion transfer channel, spatial-temporal dimensions, controlled transport, dual ion release kinetics*

INTRODUCTION

The controlled manipulation of substances within precise spatial and temporal constraints is crucial for the fundamental processes that sustain life. Biological ion channels are pivotal in maintaining cellular equilibrium, transmitting neuronal signals, and enabling muscle contractions, as they transport ions across cell membranes with remarkable efficiency and specificity.[1−3] These natural channels employ specialized selectivity filters to allow for the precise movement of ions, which is generally composed of protein sequences containing multiple continuous ion binding sites.[4−8] The unique ion translocation mechanism has inspired the creation of synthetic analogs, which has great implication in water purification and disease treatment.[9−15] To facilitate ion transport across lipid bilayers, various noncovalent interactions, such as hydrogen bonding, dipole interactions, and ion-π interactions have been incorporated, where innovation designs include unimolecular systems, self-assembled structures, and nanopore-based channels.[16−22] In addition to enhancing ion permeation rates and selectivity, a significant focus of ion channel research is the investigation of sequential ion movement across binding sites within natural selective filters.[23−26] The exact mechanism of ion permeation, however, remains a subject of debate due to its complexity.[27] Research into ion translocation in artificial systems provides valuable insights into ion dynamics, though constructing such model systems poses distinct challenges. Typically, ion binding in artificial systems with multiple binding sites occurs randomly, even when these sites are spatially connected.[28−33] Alternatively, altering the ion's valence can facilitate its translocation between binding sites with distinct recognition properties.[34,35] In contrast, achieving spatially dependent ion dislocation without altering their valence is crucial for mimicking the elementary steps that occur during the ion transfer in natural ion channels. To address these issues, we propose a novel bioinspired receptor featuring dual continuous ion coordination sites, with one situated in a confined space. This design enables selective ion recognition and facilitates ion dislocation from external to buried binding sites (Figure 1), mimicking the sequential ion binding intrinsic to natural ion channels, though without transporting ions across a membrane. By enabling controlled ion dislocation through selective interactions, this approach not only deepens our understanding of ion dislocation mechanisms but also opens the door to the development of smart supramolecular systems. These systems are characterized by nonequilibrium states and spatially controlled recognition processes. Investigations have demonstrated that this new ion receptor permits ion dislocation within a confined environment, where the transition between ion recognition states occurs sequentially rather than randomly. Notable behaviors, such as the slow release of ions and selective uptake of two distinct ions, were demonstrated.

Received: August 17, 2024
Revised: October 1, 2024
Accepted: October 2, 2024
Published: October 20, 2024

https://doi.org/10.1021/jacsau.4c00752
JACS Au 2024, 4, 4415−4422

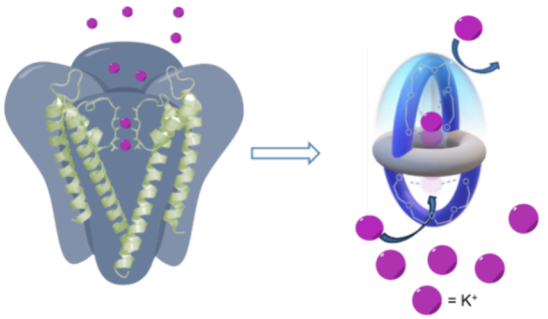

Figure 1. Design of ion host with a spatially confined ion recognition tunnel.

RESULTS AND DISCUSSION

Our research began by exploring supramolecular systems designed to accommodate multiple ions simultaneously, a feature often seen in biomacromolecules and network materials[36−40] but less explored in artificial ion hosts. This gap is especially notable in tubular systems that feature interconnected binding pockets, which enable efficient ion shuttling. A prominent example that meets these criteria is the bis-crown-ether calix[4]arene.[30,33] These molecules feature two ion binding sites and allows for ion tunneling through the channel formed by its calixarene backbone. However, the coordination sites in these systems are exposed to the surrounding solution, leading to a rapid and continuous exchange between the bound ion and free ions in solution (Figure 2a). Consequently, controlling the transition between distinct ion recognition states (Figure 2a, labeled A through D) becomes challenging. For example, the transition from state B to state C can occur via intramolecular ion tunneling or through intermolecular ion decomplexation and complexation, using state A as an intermediary. Additionally, access to a two-ion bound state can be achieved through multiple pathways: A-B-D, A-C−D, or A-D. These various pathways add complexity to the study of ion shuttling through the channel, diminishing the system's ability to mimic ion translation in biological channels effectively. To mitigate intermolecular ion exchange, our strategy involves encapsulating one crown ether moiety within a confined space while leaving the other exposed to the solution (Figure 2b). This design enables the exposed binding site in E to readily capture ions from the solution. Subsequently, the ion moves from the external crown ether moiety to the internal one via the calixarene channel. Owing to the confined binding pocket, this new ion receptor is envisioned to allow for sequential (E-F-G-H) rather than random interconversion between distinct ion recognition states, as depicted in Figure 2b. This receptor design thereby mimics the sequential interactions typical of the selectivity filter domain of biological channels but does not perform ion transport.

The target ion host was synthesized using a strategy similar to the one employed for constructing calix[4]trap,[41] a host known for differentiating ions based on binding strength and kinetic uptake rates. The synthetic pathway leverages the unique attributes of calix[4]arene, which allows for structural modifications at both the upper and lower rims, leading to significant applications across various fields.[42−46] Starting from the previously described compound **3**, we introduced a second crown ether group by reacting with $Ts(OCH_2CH_2)_4OTs$ under basic conditions in acetonitrile (Scheme 1).[47] During this reaction, the calix[4]arene structure flipped, likely due to cation-π interactions between the bound K^+ ions and the iodo-substituted aryl sidewalls.[48] Following this, Negishi coupling was utilized to attach two aryl groups with terminal alkene substituents. Ammonium ions served as template ions due to its interactions with the aromatic sidewall, which promote the conformation ideal for the ring-closing metathesis (RCM) reaction (Scheme 1).[49] ^{1}H NMR analysis of a mixture of **5** and

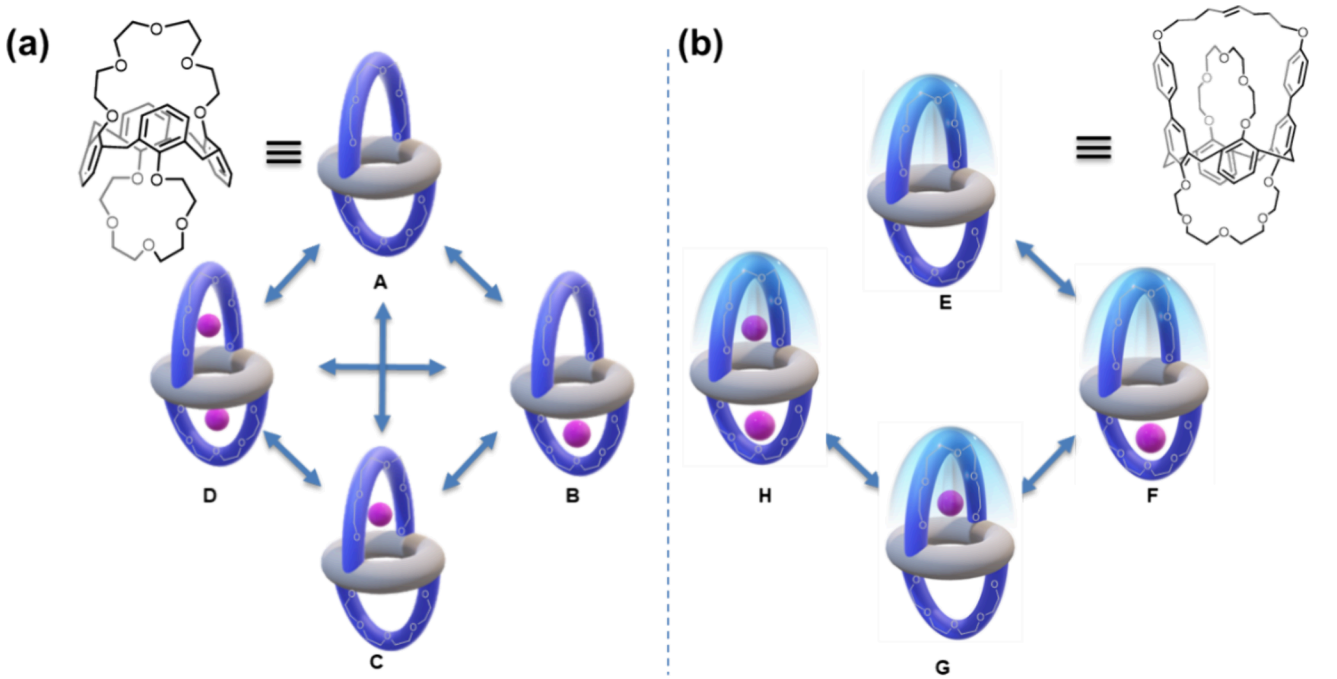

Figure 2. Comparison between ion recognition behaviors of previous and our designed ion host. (a) Recognition behavior of ions host without encapsulation of the chelating sites. (b) Recognition behavior of ions host with encapsulation of the chelating sites.

https://doi.org/10.1021/jacsau.4c00752
JACS Au 2024, 4, 4415−4422

Scheme 1. Synthetic Route for the Target Ion Host 7a

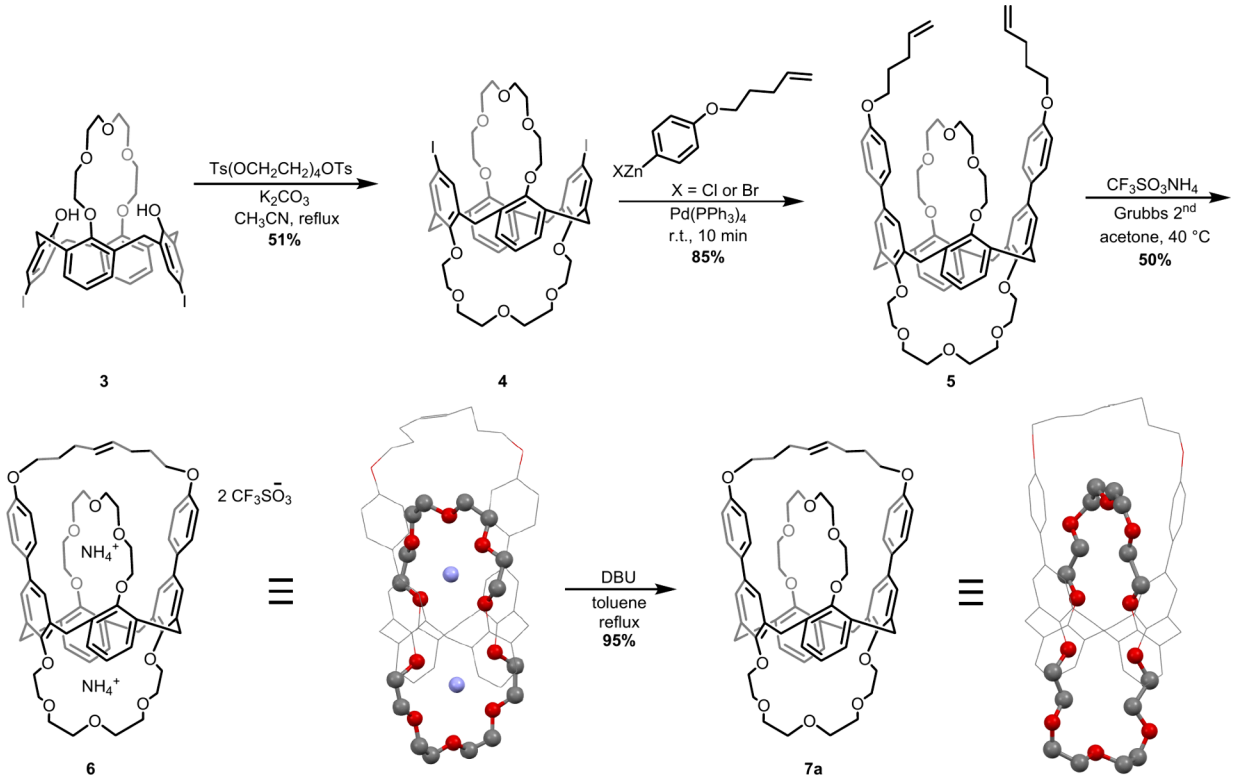

NH_4^+ revealed a pronounced downfield shift in the proton signals associated with the aromatic sidewall of **5**, supporting the occurrence of binding in solution. The X-ray single-crystal structure revealed that two ammonium ions bind at distinct sites: one exposed and the other buried (Scheme 1, **6**). Finally, removal of the ammonium ions using the organic superbase DBU in refluxed toluene yielded the desired ion host. The X-ray single-crystal structure of compound **7a** confirmed its configuration,[50] featuring two contiguous ion-binding sites, with the external crown ether moiety acting as an entry point for ions into the binding tunnel (Scheme 1).

With the target ion host **7a** in hand, we proceeded to investigate its ion-binding properties. We added varying amounts of K^+ to a solution of **7a** in a 4:1 mixture of CD_3CN and $CDCl_3$ to ensure the dissolution of both ion-free and ion-complexed forms of **7a** (Figure 3a, **7a**–**7d**). Due to the strong binding affinity of **7a** for K^+ and its confined binding cavity, the ion recognition process is slow on the NMR time scale, allowing us to identify different ion recognition states through ^{1}H NMR analysis. The ^{1}H NMR spectra revealed that, with the addition of less than one equivalent of K^+ to **7a**, three distinct species were present in the system: the uncomplexed **7a** (red), K^+ complexed at the external binding site (**7b**, green), and K^+ trapped in the buried binding site (**7c**, blue). Notably, it takes time for K^+ to enter the buried binding site, enabling us to monitor the conversion between **7b** and **7c** directly through ^{1}H NMR (Figure 3c). Although the concurrent conversion of **7a** to **7b** complicates the kinetic analysis, we estimated the ion translocation rate (conversion of **7b** to **7c**) based on the ion release rate (1.36×10^{-5} s^{-1}) and the equilibrium constant (K = 1.83, Table S2), yielding a value of 2.5×10^{-5} s^{-1}. This suggests that the kinetics of ion uptake and release are comparable, indicating a similar transition state for both processes under these conditions. Since the ion must dissociate from the external binding site before moving to the buried site, the transition likely involves a high-energy barrier, which accounts for the observed slow kinetics. Although the kinetic complexity of the system hindered the direct measurement of binding constants, ^{1}H NMR data revealed that the external binding site exhibits approximately 1.83 times stronger binding affinity compared to the buried site (Figure 3a, 0.7 equiv of K^+ added, and Table S2). Notably, the buried binding site in **7a** bears similarities to the previously reported calix[4]trap,[41] indicating comparable binding capacities. Drawing on the literature values for calix[4]trap, we estimate the binding constants for the external site ($\log K_1$) and the buried site ($\log K_2$) to be approximately 8.8 and 8.6 at 25 °C, respectively. When 1.5–2 equiv of K^+ were added, species **7a** disappeared, while species **7d** (marked in indigo), which binds with two K^+ ions, became more abundant. When more than 2 equiv of K^+ were added, species **7d** became the major component. This titration experiment indicates the following: 1) each complexation state undergoes slow interconversion, allowing clear characterization by ^{1}H NMR; 2) **7a** can complex with K^+ in a 1:1 or 1:2 ratio, with the complexation proceeding sequentially. The first K^+ ion has to enter the buried site through the channel structure before the second K^+ can coordinate to the external binding site. These observations indicate that there is a clear pathway for K^+ recognition, allowing the dislocation of K^+ from the bulk solution to the external binding site, and subsequently to the buried binding site.

The system's electronic properties changed significantly after ion complexation, causing notable shifts in the chemical shifts of the ^{1}H signals in each complexation state. For example, in the singlet ^{1}H peaks labeled 1a, 1b, 1c, and 1d, K^+ complexation exerts a deshielding effect, causing the ^{1}H NMR signals for 1a–1d to move progressively to a lower field.

https://doi.org/10.1021/jacsau.4c00752
JACS Au 2024, 4, 4415–4422

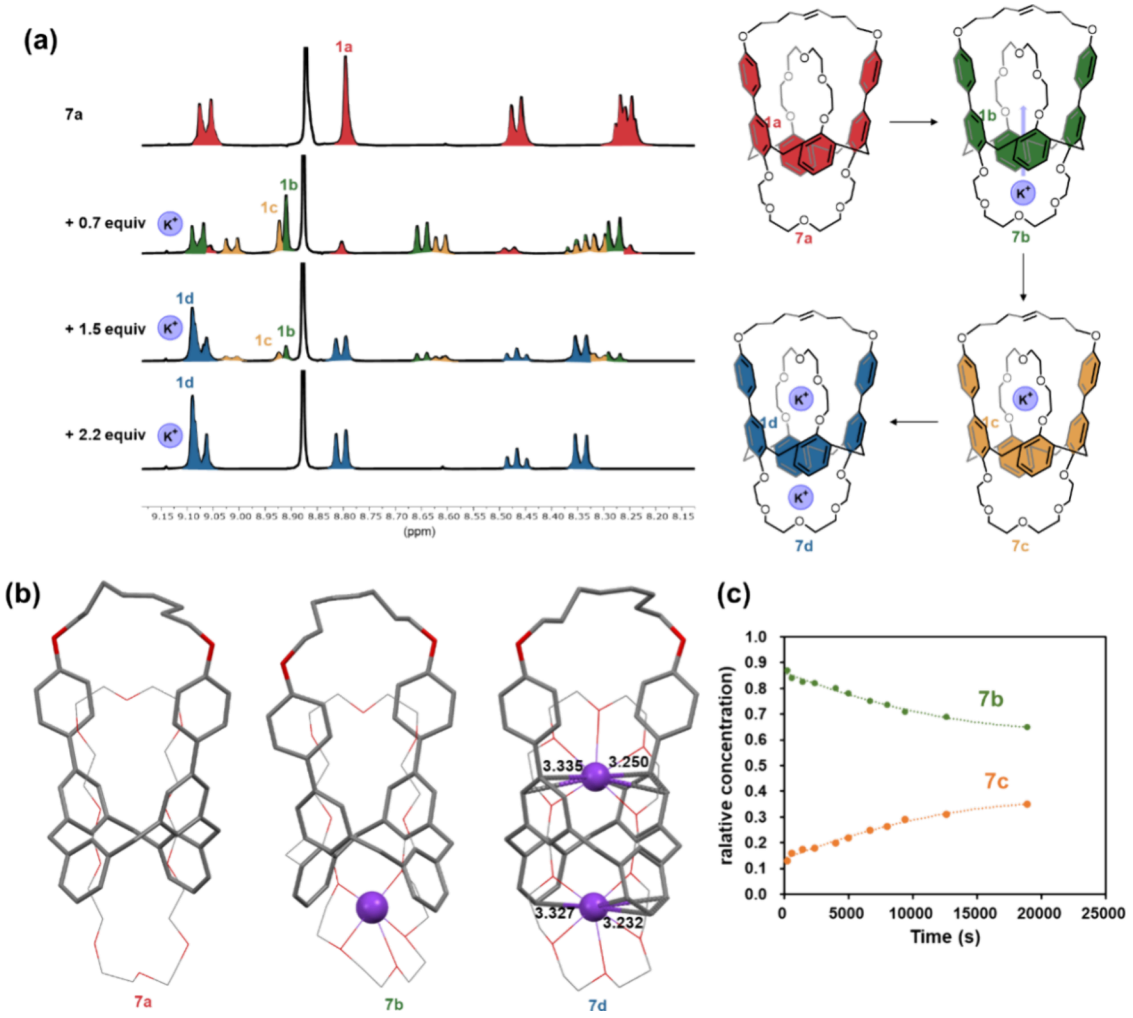

Figure 3. (a) ^{1}H NMR titrations of K^+ into a solution of **7a**. Titration was performed at 25 °C with an ion host concentration of 3 mM in CD_3CN:$CDCl_3$ = 4:1. (b) X-ray single crystal structures of **7a**, **7b**, and **7d**. (c) Changes in the relative concentrations of species **7b** and **7c** following the addition of 0.33 equiv of K^+ at 25 °C.

The NMR signal shift observed during the conversion from **7a** to **7b** is due to K^+ binding with the external crown ether moiety, which reduces the electron-donating ability of the oxygen atom to the arene. In contrast, the distinct ^{1}H NMR shifts between **7a** and **7c** is largely attributed to the cation-π interactions between the complexed K^+ and the aromatic sidewall. Notably, in **7c**, the buried crown ether moiety is not directly connected to the aromatic sidewall involved in the cation-π interaction. Therefore, the pronounced downfield shift observed in **7c** cannot be attributed solely to ion-crown ether binding. Additionally, density functional theory (DFT) calculations of the electrostatic potential energy for **7a**, **7b**, **7c**, and **7d** reveal that the energies around the flipped aromatic ring are 57, 234, 278, and 468 kJ/mol, respectively (as shown in Figure S33). The relatively small energy difference between **7b** and **7c** at this site aligns with the similar chemical shifts observed for the proton labeled 1b and 1c in Figure 3a for these two structures. As expected, the most downfield-shifted ^{1}H NMR signal was observed in **7d**, where both of the aforementioned effects are present. Notably, we successfully obtained the X-ray single crystal structures for **7a**, **7b**, and **7d** (Figure 3b),[51] where cation-π interactions were observed in **7d**. In the structure of **7d**, the distance between the ion and the flipped aromatic sidewall is approximately 3.3 Å, suggesting the presence of a cation-π interaction.[52] The growth of crystals for **7c** was not successful, likely due to its inferior stability. We next explored the recognition behavior of **7a** toward other cations. The results showed that **7a** could complex with Li^+, Na^+, K^+, Rb^+, Cs^+, NH_4^+, and $CH_3NH_3^+$ when an excess of these ions was introduced to a solution of **7a** in CD_3CN/$CDCl_3$ (v:v 1:1). Among them, Na^+, K^+, Rb^+, and NH_4^+ could achieve dual complexation to form a 1:2 complex (for details, see the NMR experiments in Figures S6 and S7 in the Supporting Information). Due to the high hydration energy of Li^+, complete dehydration to access the buried binding site is unfavorable, resulting in interactions only with the external binding site. Similarly, large ions like $CH_3NH_3^+$ cannot access the buried binding site because their steric bulkiness prevents them from passing through the channel (Figure S5 in the Supporting Information). In contrast, Cs^+, with its medium size, can still pass through the channel and bind to the buried site, although the process is quite slow. The X-ray single crystal structures depicted in Figure S32 in the Supporting Information indicate that the size of the bound ions has a significant influence on the distance between the unflipped aromatic rings around the naked crown-ether moiety.[53] As the radius of bound ions increases, the distance between these unflipped aromatic rings is continuously increasing (Figure S32

https://doi.org/10.1021/jacsau.4c00752
JACS Au 2024, 4, 4415−4422

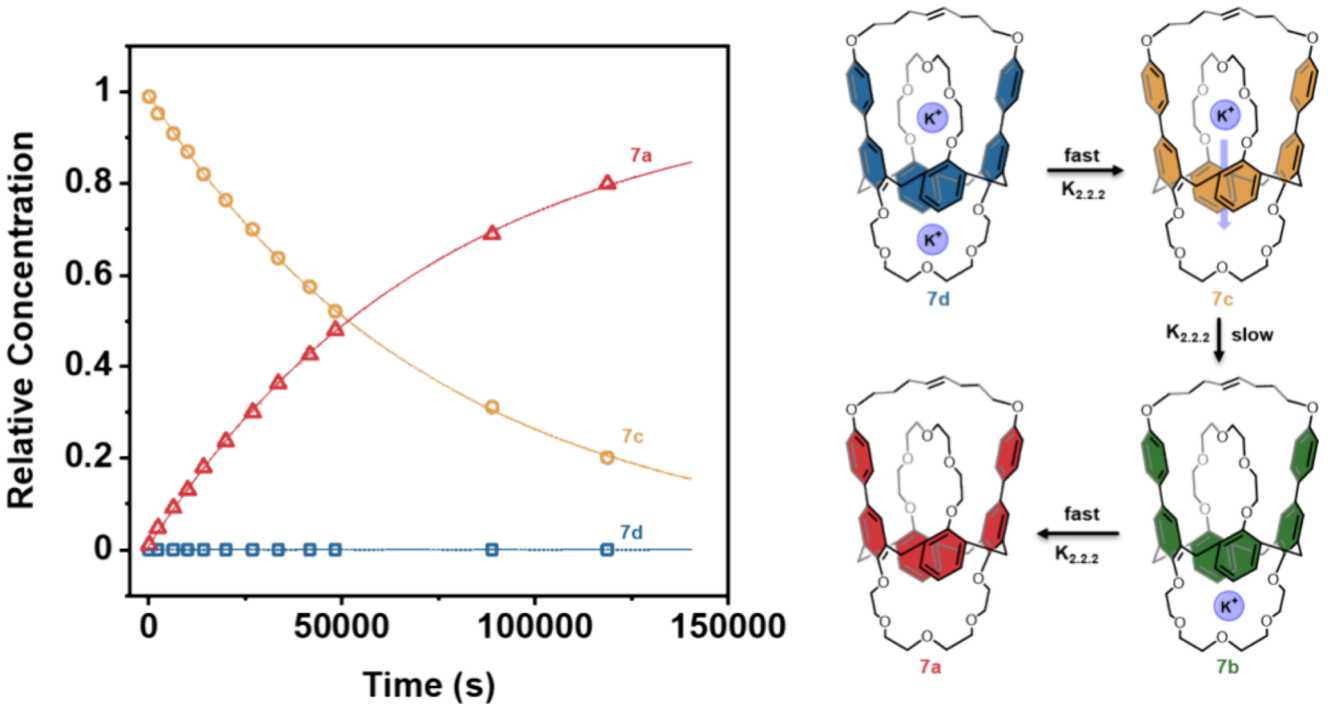

Figure 4. Kinetic study of K^+ dissociation of **7d**. The experiments were performed at 25 °C with an ion host concentration of 3 mM in CD_3CN:$CDCl_3$ = 4:1.

in the Supporting Information). These observations collectively suggest a size-dependent ion recognition selectivity.

Owing to its unique structure, the ion release behavior of this system is interesting. Although this is the reverse process of the previously discussed ion association, the kinetics may differ significantly. In these experiments, we used crypt-and[2.2.2] (K2.2.2) to trap the released K^+, preventing any rebound between **7a** and K^+. This approach allowed us to visualize the kinetic process of K^+ release. Using ^1H NMR to monitor the ion release, the experimental results showed that once K2.2.2 was added, all **7d** converted to **7c**, indicating that the K^+ complexed with the external binding site undergoes rapid chemical exchange with the free K^+ in the bulk solution (Figure 4). Over time, **7c** was gradually converted to **7a**, eventually leading to the complete release of K^+. Due to the more rapid release of K^+ at the external binding site compared to the buried one, we did not observe the generation of **7b** during the ion release process (Figure 4). The K^+ release from the buried site was found to follow first-order kinetics, which is not affected by the amount of K2.2.2 added (Table S7 in the Supporting Information). Additionally, we used K2.2.2 to measure the dissociation rates of Rb^+ and NH_4^+ from the buried binding site. The calculated dissociation rate constant for Rb^+ was 2.66×10^{-6} s^{-1}, which was lower than that of K^+. The dissociation rate constant for NH_4^+ was 1.50×10^{-5} s^{-1}, situated between those of K^+ and Rb^+ (Figures S21 and S24 in the Supporting Information). This result demonstrates a correlation between the dissociation rate and the ion radius: as the size of the ion increases, it becomes more difficult for the ion to pass through the channel, thereby impeding the ion release process. Collectively, the observations indicate that ion release occurs successively, with the K^+ bound to the external binding site releasing more rapidly compared to that trapped inside. This dual ion release behavior may have important implications for ion regulation in complex systems. For instance, when the concentration of K^+ in the external environment decreases, the externally coordinated K^+ can be readily released to rapidly compensate for the K^+ shortage. If the K^+ shortage persists, the buried K^+ undergoes slow release, ensuring a prolonged K^+ supply and increasing the system's ability to resist environmental stress.

To further demonstrate the unique property of **7a**, which possesses continuous binding sites, including one buried inside the tunnel structure, we attempted to prepare an ion host bound with two different ions selectively. We selected ^{15}N-labeled ammonium ions ($^{15}NH_4^+$) as one of the ions for investigation because its complexation with **7a** can be clearly analyzed and interpreted using NMR spectroscopy. The J coupling between ^1H and ^{15}N allows for easy identification of the ^1H in $^{15}NH_4^+$ in both free and complex states. Furthermore, unambiguous analysis can be performed using 1D $^{15}N-^1H$ Heteronuclear Single Quantum Coherence (1D $^{15}N-^1H$ HSQC) spectroscopy, where the simplified spectra enable the identification of tiny variations in the ion recognition process. Initially, we incorporated 0.5 equiv of $^{15}NH_4^+$ into the system. Utilizing 1D $^{15}N-^1H$ HSQC spectroscopy, we confirmed that the hydrogen atoms of the ammonium ions, whether coordinated at external binding site or buried binding site, exhibit two similar chemical shifts in the vicinity of 3.8 ppm (Figure S34 in the Supporting Information). In the designed experiment, 2.0 equiv of $^{15}NH_4^+$ were mixed with **7a** to obtain **7e** containing two bound $^{15}NH_4^+$ ions (Figure 5, **7e**). Subsequently, 1.2 equiv of K^+ were added. Due to the higher affinity of K^+ compared to $^{15}NH_4^+$ for the external binding site and the rapid ion exchange kinetics, the externally bound $^{15}NH_4^+$ was selectively replaced by K^+, resulting in **7f** with $^{15}NH_4^+$ and K^+ bound to the buried and external binding sites, respectively (Figure 5, **7f**). This process is supported by ^1H NMR analysis. The characteristic ^1H NMR signals for free $^{15}NH_4^+$ appear at δ 7.32 with J = 73.6

https://doi.org/10.1021/jacsau.4c00752
JACS Au 2024, 4, 4415−4422

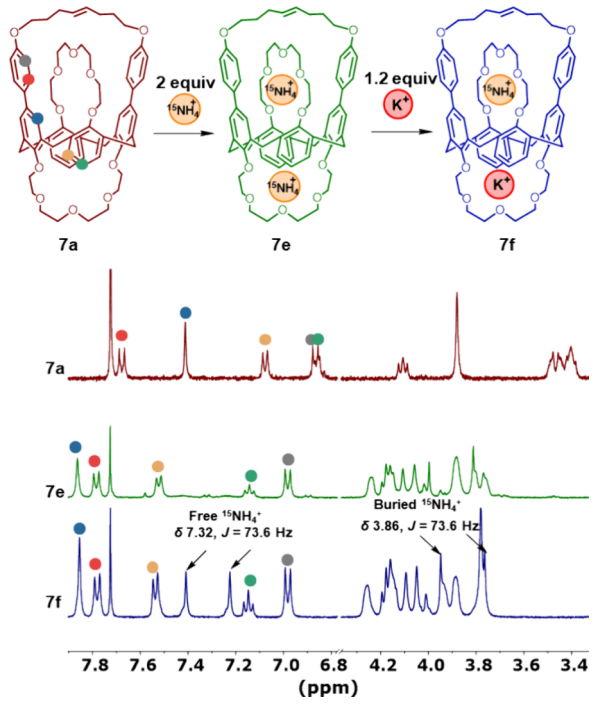

Figure 5. Selective binding of two different ions using **7a** in acetone-d_6:$CDCl_3$ = 1:1.

Hz, while the signals for the retained $^{15}NH_4^+$ appear at δ 3.86 with J = 73.6 Hz (Figure 5, **7f**). Additionally, the $^1H-^1H$ rotating-frame Overhauser effect spectroscopy (ROESY) experiment further supports the localization of $^{15}NH_4^+$ in the buried binding site (Figure S35, Supporting Information). These observations confirm the formation of **7f**, where different ions are selectively positioned in the anticipated binding sites. Notably, this recognition behavior contrasts sharply with ion hosts that have only open binding sites, where both $^{15}NH_4^+$ ions would be replaced immediately. We further investigated the potential of constructing a reverse configuration, with $^{15}NH_4^+$ positioned at the external binding site and K^+ occupying the buried site. To achieve this, varying amounts of $^{15}NH_4^+$ were introduced to an ion host preloaded with two K^+ ions. As the concentration of $^{15}NH_4^+$ increased, it selectively bound to the external site, partially displacing K^+, while the buried K^+ remained unaffected (Figures S36 and S37 in the Supporting Information). These findings highlight the unique ion recognition capabilities of this system, which incorporates continuous binding sites within a confined environment.

CONCLUSIONS

In summary, we explored the distinctive ion recognition capabilities of a bioinspired ion host featuring a continuous array of binding sites, including one deeply embedded within a tunnel-like structure. The process of ion uptake and release occurs as ions translocation from one binding site to another in a controlled and sequential manner. This movement is governed by the spatial constraints and the tunnel structure, effectively replicating the ion dislocation steps observed in the selectivity filters of natural ion channels. Unlike systems with solely open binding sites, this bioinspired model allows for a sequential interconversion between different ion recognition states, rather than a random exchange. Additionally, this approach revealed novel properties such as dual ion release kinetics, suggesting its potential effectiveness in regulating ion balance in complex physiological conditions and responding adaptively to environmental changes. We further delved into the selective binding of two different ions, which poses a challenge in systems with only open binding sites. We expect that the construction of effective mimics of natural ion channels would set the foundation for future innovations in this field, paving the way for the development of materials specifically engineered for tailored ion regulation.

METHODS

Procedure for the Synthesis of Calixarene Derivative 4

A solution of 11,23-diiodo-25,27-dihydroxycalix[4]arenecrown-5 (**3**) (1.20 g, 1.43 mmol, 1.0 equiv) and K_2CO_3 (0.60 g, 15.80 mmol, 2.5 equiv) in acetonitrile (200 mL) was prepared. To this, tetraethylene glycol ditosylate (0.72 g, 4.74 mmol, 1.0 equiv) was added, and the mixture was refluxed at 125 °C for 5 h. Progress of the reaction was monitored by UPLC and TLC. Upon completion, the acetonitrile was evaporated, and the residue was dissolved in dichloromethane. The resulting solution was passed through a short column of basic alumina. The filtrate was collected, evaporated, and purified by silica gel column chromatography using a petroleum ether/ethyl acetate mixture as the eluent, affording product **4** as a white solid (0.72 g, 0.73 mmol, 51% yield).

Procedure for the Synthesis of Calixarene Derivative 5

1-Bromo-4-(pent-4-en-1-yloxy)benzene (0.60 g, 2.40 mmol, 1.0 equiv) was added to a 25 mL round-bottom flask, which was degassed and purged with nitrogen three times. Anhydrous THF (2.0 mL) was added, and the reaction mixture was cooled to −78 °C using a dry ice-acetone bath. A solution of n-BuLi in hexane (1.8 mL, 1.6 M, 2.88 mmol, 1.2 equiv) was then added dropwise, followed by a solution of $ZnCl_2$ in THF (3.6 mL, 1.0 M, 3.6 mmol, 1.5 equiv). The reaction was stirred for 10 min at −78 °C. After removing the cooling bath, calix[4]arene derivative **4** (581 mg, 0.59 mmol, 0.25 equiv) and $Pd(PPh_3)_4$ (68 mg, 58.6 μmol, 10 mol % relative to compound **4**) were added to the reaction mixture. The reaction was stirred at room temperature for 30 min. Once the reaction was complete, as confirmed by UPLC and TLC, water was added to quench the reaction. The mixture was diluted with ethyl acetate, and the organic phase was washed with water and brine. The solvent was removed under reduced pressure, and the crude product was purified by silica gel column chromatography using a mixture of petroleum ether and ethyl acetate as the eluent. This process yielded calixarene derivative **5** as a white solid (532 mg, 0.50 mmol, 85% yield).

Procedure for the Synthesis of Ion Host 7a

Calixarene derivative **5** (0.93 g, 0.88 mmol, 1.0 equiv) and ammonium trifluoromethanesulfonate (0.44 g, 2.63 mmol, 3.0 equiv) were dissolved in 500 mL of acetone, and the solution was purged with nitrogen for 10 min to remove any dissolved oxygen. Grubbs second generation catalyst (75 mg, 87.8 μmol, 10 mol %) was then added to the mixture. The reaction was heated to 40 °C under a nitrogen atmosphere and stirred for 5 h. Upon completion of the reaction, as confirmed by UPLC and TLC, ethyl vinyl ether (0.5 mL) was added, and the reaction was allowed to proceed at room temperature for an additional 30 min. The solvent was removed under reduced pressure using rotary evaporation. The resulting crude product was first purified via silica gel column chromatography using a petroleum ether/ethyl acetate mixture as the eluent. Further purification was carried out via reverse-phase column chromatography (C_{18}, 20−45 μm) with a methanol/water mixture as the eluent, yielding compound **6** as a white solid (yield: 50%, 601 mg, 0.44 mmol). Compound **6** was then treated with 0.5 mL of DBU in refluxing toluene for 30 min. Afterward, the solvent was removed via rotary evaporation. The resulting material was washed with cold

https://doi.org/10.1021/jacsau.4c00752
JACS Au 2024, 4, 4415−4422

methanol (3x) to yield ion host **7a** as a white solid (yield calculated from compound **6**: 95%, 431 mg, 0.42 mmol).

■ ASSOCIATED CONTENT

Supporting Information

The Supporting Information is available free of charge at https://pubs.acs.org/doi/10.1021/jacsau.4c00752.

Synthesis and characterization of all compounds, and procedures for NMR experiments (PDF)

X-ray single crystal structures (ZIP)

■ AUTHOR INFORMATION

Corresponding Author

Yanchuan Zhao − *Key Laboratory of Fluorine and Nitrogen Chemistry and Advanced Materials, Shanghai Institute of Organic Chemistry, University of Chinese Academy of Sciences, Chinese Academy of Sciences, Shanghai 200032, China;* orcid.org/0000-0002-2903-4218; Email: zhaoyanchuan@sioc.ac.cn

Authors

Wenjie Zhu − *Key Laboratory of Fluorine and Nitrogen Chemistry and Advanced Materials, Shanghai Institute of Organic Chemistry, University of Chinese Academy of Sciences, Chinese Academy of Sciences, Shanghai 200032, China*

Zhenchuang Xu − *Key Laboratory of Fluorine and Nitrogen Chemistry and Advanced Materials, Shanghai Institute of Organic Chemistry, University of Chinese Academy of Sciences, Chinese Academy of Sciences, Shanghai 200032, China*

Wei Zhang − *Key Laboratory of Fluorine and Nitrogen Chemistry and Advanced Materials, Shanghai Institute of Organic Chemistry, University of Chinese Academy of Sciences, Chinese Academy of Sciences, Shanghai 200032, China*

Qi Jia − *Key Laboratory of Fluorine and Nitrogen Chemistry and Advanced Materials, Shanghai Institute of Organic Chemistry, University of Chinese Academy of Sciences, Chinese Academy of Sciences, Shanghai 200032, China*

Haoliang Hao − *Key Laboratory of Fluorine and Nitrogen Chemistry and Advanced Materials, Shanghai Institute of Organic Chemistry, University of Chinese Academy of Sciences, Chinese Academy of Sciences, Shanghai 200032, China*

Yucheng Gu − *Jealott's Hill International Research Centre, Syngenta, Bracknell RG42 6EY, U.K.;* orcid.org/0000-0002-6400-6167

Complete contact information is available at: https://pubs.acs.org/10.1021/jacsau.4c00752

Notes

The authors declare no competing financial interest.

■ ACKNOWLEDGMENTS

This work was supported by the National Natural Science Foundation of China (Nos. 22271305), Strategic Priority Research Program of the Chinese Academy of Science (XDB0590000), and the Syngenta Ph.D. fellowship (W.Z.). We thank the staff at BL17B1 beamline of the National Facility for Protein Science in Shanghai (NFPS), Shanghai Advanced Research Institute, CAS, for providing technical support in X-ray diffraction data collection and analysis. The authors thank Professor Yanming Wang and Yide Chang from Jiaotong University for help discussion.

■ REFERENCES

(1) Wray, D. Structure and Function of Ion Channels. *Eur. Biophys. J.* **2009**, *38*, 271−272.

(2) Dubyak, G. R. Ion Homeostasis, Channels, and Transporters: An Update on Cellular Mechanisms. *Adv. Physiol. Educ.* **2004**, *28*, 143−154.

(3) Feske, S.; Skolnik, E.; Prakriya, M. Ion channels and transporters in lymphocyte function and immunity. *Nat. Rev. Immunol.* **2012**, *12*, 532−547.

(4) Doyle, D. A.; Cabral, J. M.; Pfuetzner, R. A.; Kuo, A.; Gulbis, J. M.; Cohen, S. L.; Chait, B. T.; MacKinnon, R. The Structure of the Potassium Channel: Molecular Basis of K^+ Conduction and Selectivity. *Science* **1998**, *280*, 69−77.

(5) Zhou, Y.; Morais-Cabral, J. H.; Kaufman, A.; Mackinnon, R. Chemistry of Ion Coordination and Hydration Revealed by a K^+ Channel-Fab Complex at 2.0 Å Resolution. *Nature* **2001**, *414*, 43−48.

(6) Matamoros, M.; Ng, X. W.; Brettmann, J. B.; Piston, D. W.; Nichols, C. G. Conformational Plasticity of NaK2K and TREK2 Potassium Channel Selectivity Filters. *Nat. Commun.* **2023**, *14*, 89.

(7) Stevens, M. J.; Rempe, S. L. B. Insight into the K Channel's Selectivity from Binding of K^+, Na^+ and Water to N-Methylacetamide. *Faraday Discuss.* **2024**, *249*, 195−209.

(8) MacKinnon, R. Potassium Channels and the Atomic Basis of Selective Ion Conduction (Nobel Lecture). *Angew. Chem., Int. Ed.* **2004**, *43*, 4265−4277.

(9) Shen, J.; Liu, G.; Han, Y.; Jin, W. Artificial channels for confined mass transport at the sub-nanometre scale. *Nat. Rev. Mater.* **2021**, *6*, 294−312.

(10) Ghahari, A.; Farzad, F.; Azadnejad, R. The strategy of three-dimensional Covalent Organic Frameworks to exclude dye contaminants in aqueous solutions. *npj Clean Water* **2024**, *7*, 27.

(11) Ling, Q. H.; Fu, Y.; Lou, Z. C.; Yue, B.; Guo, C.; Hu, X.; Lu, W.; Hu, L.; Wang, W.; Zhang, M.; Yang, H. B.; Xu, L. Naphthalene Diimide-Based Metallacage as an Artificial Ion Channel for Chloride Ion Transport. *Adv. Sci.* **2024**, *11*, No. 2308181.

(12) Yang, J.; Yu, G.; Sessler, J. L.; Shin, I.; Gale, P. A.; Huang, F. Artificial Transmembrane Ion Transporters as Potential Therapeutics. *Chem.* **2021**, *7*, 3256−3291.

(13) Zaydman, M. A.; Silva, J. R.; Cui, J. Ion Channel Associated Diseases: Overview of Molecular Mechanisms. *Chem. Rev.* **2012**, *112*, 6319−6333.

(14) Bagal, S. K.; Brown, A. D.; Cox, P. J.; Omoto, K.; Owen, R. M.; Pryde, D. C.; Sidders, B.; Skerratt, S. E.; Stevens, E. B.; Storer, R. I.; Swain, N. A. Ion Channels as Therapeutic Targets: A Drug Discovery Perspective. *J. Med. Chem.* **2013**, *56*, 593−624.

(15) Yan, Z. J.; Wang, D.; Ye, Z.; Fan, T.; Wu, G.; Deng, L.; Yang, L.; Li, B.; Liu, J.; Ma, T.; Dong, C.; Li, Z. T.; Xiao, L.; Wang, Y.; Wang, W.; Hou, J. L. Artificial Aquaporin That Restores Wound Healing of Impaired Cells. *J. Am. Chem. Soc.* **2020**, *142*, 15638−15643.

(16) Hou, X.; Guo, W.; Xia, F.; Nie, F. Q.; Dong, H.; Tian, Y.; Wen, L.; Wang, L.; Cao, L.; Yang, Y.; Xue, J.; Song, Y.; Wang, Y.; Liu, D.; Jiang, L. A Biomimetic Potassium Responsive Nanochannel: G-Quadruplex DNA Conformational Switching in a Synthetic Nanopore. *J. Am. Chem. Soc.* **2009**, *131*, 7800−7805.

(17) Legrand, Y. M.; Barboiu, M. Self-Assembled Supramolecular Channels: Toward Biomimetic Materials for Directional Translocation. *Chem. Rec.* **2013**, *13*, 524−538.

(18) Saha, T.; Gautam, A.; Mukherjee, A.; Lahiri, M.; Talukdar, P. Chloride Transport through Supramolecular Barrel-Rosette Ion Channels: Lipophilic Control and Apoptosis-Inducing Activity. *J. Am. Chem. Soc.* **2016**, *138*, 16443−16451.

(19) Yan, Z. J.; Li, Y. W.; Yang, M.; Fu, Y. H.; Wen, R.; Wang, W.; Li, Z. T.; Zhang, Y.; Hou, J. L. Voltage-Driven Flipping of Zwitterionic Artificial Channels in Lipid Bilayers to Rectify Ion Transport. *J. Am. Chem. Soc.* **2021**, *143*, 11332−11336.
(20) Zheng, S. P.; Huang, L. B.; Sun, Z.; Barboiu, M. Self-Assembled Artificial Ion-Channels toward Natural Selection of Functions. *Angew. Chem., Int. Ed.* **2021**, *60*, 566−597.
(21) Huang, W. L.; Wang, X. D.; Ao, Y. F.; Wang, Q. Q.; Wang, D. X. An Artificial Single Molecular Channel Showing High Chloride Transport Selectivity and pH-Responsive Conductance. *Angew. Chem., Int. Ed.* **2023**, *62*, No. e202302198.
(22) Fu, Y. H.; Hu, Y. F.; Lin, T.; Zhuang, G. W.; Wang, Y. L.; Chen, W. X.; Li, Z. T.; Hou, J. L. Constructing Artificial Gap Junctions to Mediate Intercellular Signal and Mass Transport. *Nat. Chem.* **2024**, *16*, 1418−1426.
(23) Linsdell, P. Anion Conductance Selectivity Mechanism of the CFTR Chloride Channel. *Biochim. Biophys. Acta - Biomembr.* **2016**, *1858*, 740−747.
(24) Kopec, W.; Köpfer, D. A.; Vickery, O. N.; Bondarenko, A. S.; Jansen, T. L. C.; de Groot, B. L.; Zachariae, U. Direct Knock-on of Desolvated Ions Governs Strict Ion Selectivity in K^+ Channels. *Nat. Chem.* **2018**, *10*, 813−820.
(25) Carvalho-de-Souza, J. L.; Saponaro, A.; Bassetto, C. A. Z. Jr.; Rauh, O.; Schroeder, I.; Franciolini, F.; Catacuzzeno, L.; Bezanilla, F.; Thiel, G.; Moroni, A. Experimental Challenges in Ion Channel Research: Uncovering Basic Principles of Permeation and Gating in Potassium Channels. *Adv. Phys.: X* **2022**, *7*, No. 1978317.
(26) Wang, S.; Lee, S. J.; Maksaev, G.; Fang, X.; Zuo, C.; Nichols, C. G. Potassium Channel Selectivity Filter Dynamics Revealed by Single-Molecule FRET. *Nat. Chem. Biol.* **2019**, *15*, 377−383.
(27) Mironenko, A.; Zachariae, U.; de Groot, B. L.; Kopec, W. The Persistent Question of Potassium Channel Permeation Mechanisms. *J. Mol. Biol.* **2021**, *433*, No. 167002.
(28) Ju, H.; Habata, Y.; Jung, J. H.; Lee, S. S. Coordinative Networking of Thiacalix[4]-Bis-Monothiacrown-5 with Hard, Borderline, and Soft Metal Salts via Exo- And Endo/Exo-Coordination. *Cryst. Growth Des.* **2021**, *21*, 6992−7001.
(29) Kim, J. S.; Lee, W. K.; Suh, I. H.; Kim, J. G.; Yoon, J.; Lee, J. H. Heterogeneous Binuclear Complexation of 1,3-Alternate Calix[4]-Bis-Crown Bearing Two Different Crown Rings. *J. Org. Chem.* **2000**, *65*, 7215−7217.
(30) Ikeda, A.; Tsudera, T.; Shinkai, S. Molecular Design of a "Molecular Syringe" Mimic for Metal Cations Using a 1,3-Alternate Calix[4]arene Cavity. *J. Org. Chem.* **1997**, *62*, 3568−3574.
(31) Lee, J. Y.; Kim, H. J.; Park, C. S.; Sim, W.; Lee, S. S. A Calix-Bis-Crown with Hard and Soft Crown Cavities: Heterobinuclear K^+/Ag^+ Complexation in Solid and Solution States. *Chem. - Eur. J.* **2009**, *15*, 8989−8992.
(32) Koh, K. N.; Araki, K.; Shinkai, S.; Asfari, Z.; Vicens, J. Cation Binding Properties of a Novel 1,3-Alternate Calix[4]Biscrown. Formation of 1:1 and 1:2 Complexes and Unique Cation Tunneling across a Calix[4]Arene Cavity. *Tetrahedron Lett.* **1995**, *36*, 6095−6098.
(33) Kim, J. S.; Yang, S. H.; Rim, J. A.; Kim, J. Y.; Vicens, J.; Shinkai, S. Silver Ion Oscillation through Calix[4]Azacrown Tube. *Tetrahedron Lett.* **2001**, *42*, 8047−8050.
(34) Zelikovlch, L.; Libman, J.; Shanzer, A. Molecular redox switches based on chemical triggering of iron translocation in triple- stranded helical complexes. *Nature* **1995**, *374*, 790−792.
(35) Sadhu, K. K.; Bharadwaj, P. K. Translocation of Copper within the Cavity of Cryptands: Reversible Fluorescence Signaling. *Chem. Commun.* **2008**, *35*, 4180−4182.
(36) Liang, X.; Tian, Y.; Yuan, Y.; Kim, Y. Ionic Covalent Organic Frameworks for Energy Devices. *Adv. Mater.* **2021**, *33*, No. 2105647.
(37) Zhang, P.; Wang, Z.; Cheng, P.; Chen, Y.; Zhang, Z. Design and Application of Ionic Covalent Organic Frameworks. *Coord. Chem. Rev.* **2021**, *438*, No. 213873.
(38) Li, X.; Xu, H. S.; Leng, K.; Chee, S. W.; Zhao, X.; Jain, N.; Xu, H.; Qiao, J.; Gao, Q.; Park, I. H.; Quek, S. Y.; Mirsaidov, U.; Loh, K. P. Partitioning the Interlayer Space of Covalent Organic Frameworks by Embedding Pseudorotaxanes in Their Backbones. *Nat. Chem.* **2020**, *12*, 1115−1122.
(39) Gu, X.; Wang, B.; Pang, Y.; Zhu, H.; Wang, R.; Chen, T.; Li, Y.; Yan, X. Crown ether-based covalent organic frameworks for CO_2 fixation. *New J. Chem.* **2023**, *47*, 2040−2044.
(40) An, S.; Lu, C.; Xu, Q.; Lian, C.; Peng, C.; Hu, J.; Zhuang, X.; Liu, H. Constructing Catalytic Crown Ether-Based Covalent Organic Frameworks for Electroreduction of CO_2. *ACS Energy Lett.* **2021**, *6*, 3496−3502.
(41) Xu, Z.; Fang, N.; Zhao, Y. Calix[4]Trap: A Bioinspired Host Equipped with Dual Selection Mechanisms. *J. Am. Chem. Soc.* **2021**, *143*, 3162−3168.
(42) Pan, Y. C.; Tian, J. H.; Guo, D. S. Molecular Recognition with Macrocyclic Receptors for Application in Precision Medicine. *Acc. Chem. Res.* **2023**, *56*, 3626−3639.
(43) Yao, S. Y.; Ying, A. K.; Jiang, Z. T.; Cheng, Y. Q.; Geng, W. C.; Hu, X. Y.; Cai, K.; Guo, D. S. Single Molecular Nanomedicines Based on Macrocyclic Carrier-Drug Conjugates for Concentration-Independent Encapsulation and Precise Activation of Drugs. *J. Am. Chem. Soc.* **2024**, *146*, 14203−14212.
(44) Ding, Y.; Memon, W. A.; Zhang, D.; Zhu, Y.; Xiong, S.; Wang, Z.; Liu, J.; Li, H.; Lai, H.; Shao, M.; He, F. Dimerized Acceptors with Conjugate-Break Linker Enable Highly Efficient and Mechanically Robust Organic Solar Cells. *Angew. Chem., Int. Ed.* **2024**, *63*, No. e202403139.
(45) Zhao, Y.; Markopoulos, G.; Swager, T. M. ^{19}F NMR Fingerprints: Identification of Neutral Organic Compounds in a Molecular Container. *J. Am. Chem. Soc.* **2014**, *136*, 10683−10690.
(46) Zhu, W.; Xu, Z.; Gu, Y. C.; Zhao, Y. Research Progress on Organic Cation Receptors Based on Molecular Containers. *Chin. J. Org. Chem.* **2023**, *43*, 2991−3005.
(47) Kang, S. M.; Kim, C. H.; Lee, K. C.; Kim, D. W. Bis-Triethylene Glycolic Crown-5-Calix[4]Arene: A Promoter of Nucleophilic Fluorination Using Potassium Fluoride. *Org. Lett.* **2019**, *21*, 3062−3066.
(48) Duta, M.; Asfari, Z.; Hagege, A.; Thuery, P.; Leroy, M. Synthesis and Complexation Studies of Various Precursors Based on Calix[4]Arene-Crown-5 and −6 for the Immunoanalysis of Potassium and Caesium Ions. *Supramol. Chem.* **2004**, *16*, 205−215.
(49) Yu, M.; Lou, S.; Gonzalez-Bobes, F. Ring-Closing Metathesis in Pharmaceutical Development: Fundamentals, Applications, and Future Directions. *Org. Process Res. Dev.* **2018**, *22*, 918−946.
(50) Deposition Numbers 2263209 (**6**) and 2373273 (**7a**) contain the supplementary crystallographic data for this paper. These data are provided free of charge by the joint Cambridge Crystallographic Data Centre and Fachinformationszentrum Karlsruhe Access Structures service.
(51) Deposition Numbers 2373274 (**7b**), and 2373275 (**7c**) contain the supplementary crystallographic data for this paper. These data are provided free of charge by the joint Cambridge Crystallographic Data Centre and Fachinformationszentrum Karlsruhe Access Structures service.
(52) Mahadevi, A. S.; Sastry, G. N. Cation-π Interaction: Its Role and Relevance in Chemistry, Biology, and Material Science. *Chem. Rev.* **2013**, *113*, 2100−2138.
(53) Deposition Number 2132946 (**7a·Rb**$^+$) and 2373277 (**7a·Cs**$^+$) contain the supplementary crystallographic data for this paper. These data are provided free of charge by the joint Cambridge Crystallographic Data Centre and Fachinformationszentrum Karlsruhe Access Structures service.

https://doi.org/10.1021/jacsau.4c00752
JACS Au 2024, 4, 4415−4422